Cell, Vol. 110, 599–611, September 6, 2002, Copyright ©2002 by Cell Press

Global Conformational Rearrangements in Integrin Extracellular Domains in Outside-In and Inside-Out Signaling

Junichi Takagi,[1] Benjamin M. Petre,[2] Thomas Walz,[2] and Timothy A. Springer[1,3]
[1]The Center for Blood Research
Departments of Pathology and Pediatrics
Harvard Medical School
Boston, Massachusetts 02115
[2]Department of Cell Biology
Harvard Medical School
Boston, Massachusetts 02115

Summary

How ligand binding alters integrin conformation in outside-in signaling, and how inside-out signals alter integrin affinity for ligand, have been mysterious. We address this with electron microscopy, physicochemical measurements, mutational introduction of disulfides, and ligand binding to αVβ3 and αIIbβ3 integrins. We show that a highly bent integrin conformation is physiological and has low affinity for biological ligands. Addition of a high affinity ligand mimetic peptide or Mn^{2+} results in a switchblade-like opening to an extended structure. An outward swing of the hybrid domain at its junction with the I-like domain shows conformational change within the headpiece that is linked to ligand binding. Breakage of a C-terminal clasp between the α and β subunits enhances Mn^{2+}-induced unbending and ligand binding.

Introduction

Integrins use bidirectional signaling to integrate the intracellular and extracellular environments. In outside-in signaling, ligand binding activates intracellular signaling pathways (Giancotti and Ruoslahti, 1999; Schwartz and Ginsberg, 2002). In inside-out signaling, signals received by other receptors activate intracellular signaling pathways that impinge on integrin cytoplasmic domains, and make the extracellular domain competent for ligand binding on a time-scale of less than 1 s (Hughes and Pfaff, 1998; Shimaoka et al., 2002). These signaling pathways expose activation-dependent or ligand-induced binding site (LIBS) epitopes in integrin extracellular domains, and may also regulate integrin clustering (Bazzoni and Hemler, 1998). How conformational signals are communicated in integrins remains unknown, despite two recent watershed crystal structures of the integrin αVβ3 (Xiong et al., 2001, 2002). Both crystals were obtained in Ca^{2+}, a cation that stabilizes integrins in the inactive or low affinity conformation. It had been expected based on previous electron micrographs that integrins would have an extended conformation (Du et al., 1993; Nermut et al., 1988; Takagi et al., 2001). However, the crystal structures revealed an unexpected bent conformation, in which the headpiece is folded over the tailpiece, with each leg bent at a "genu" or knee (Figure 1). The extreme bend causes the ligand binding site in the headpiece to come down close to the C-terminal, membrane-proximal end of the two legs.

The bent conformation found in crystal lattices was suggested to be less likely to be present on cell surfaces (Xiong et al., 2001). However, extensive interfaces between the headpiece and tailpiece and between the α and β subunits in the tailpiece stabilize the bent conformation (see Discussion). Furthermore, an NMR structure of β2 integrin domains not resolved in the crystal structure (Beglova et al., 2002) showed that epitopes that become exposed when integrins are activated (Lu et al., 2001a) are buried in the bent conformation, and that β2 subunit residues that interact with the α subunit to restrain activation (Zang and Springer, 2001) are indeed in an interface with α in the bent conformation. It therefore was suggested that the bent conformation represents an inactive, physiologically relevant conformation and that activation would be accompanied by a switchblade-like opening of the headpiece-tailpiece interface (Beglova et al., 2002).

Although it was suggested that the ligand binding domains in the αVβ3 crystal structure were in an active conformation (Xiong et al., 2001), adoption of the bent conformation on the cell surface would orient the ligand binding site toward the membrane (Figure 1), a topology unfavorable for binding of ligands in the extracellular matrix or on the surface of other cells. Recently, the αVβ3 crystals have been soaked in Mn^{2+}, a cation that generally activates integrins, and a high-affinity cyclic peptide containing the ligand-mimetic Arg-Gly-Asp (RGD) motif (Xiong et al., 2002). The peptide binds with its Arg contacting the α subunit/β propeller domain and its Asp ligated to a Mn^{2+} held in the metal ion-dependent adhesion site (MIDAS) of the β subunit I-like domain. However, compared to the unligated structure, the structural changes were relatively small and were limited to the vicinity of the ligand binding site, providing no mechanism for propagating signals in outside-in or inside-out signaling.

Some integrin α subunits (but not αV) contain an I domain, which is structurally related to the I-like domain, and is the ligand binding site of those integrins that contain it. In this subset of integrins, ligand binding at the MIDAS of the I domain is activated by a 10 Å downward movement of its C-terminal α helix, which causes a rearrangement of metal ion coordination at the MIDAS, and a dramatic increase in affinity (Shimaoka et al., 2002). However, when peptide ligand was soaked into crystals containing the bent αVβ3 conformation, no rearrangement of residues in the MIDAS or C-terminal α helix movement of the I-like domain analogous to that seen in I domains was observed (Xiong et al., 2002).

It has been suggested that the peptide-αVβ3 complex in the crystal structure represents the active integrin conformation, and that activation of I and I-like domains are not analogous (Xiong et al., 2002). However, binding to peptide antagonists does not signify that a conformation has high affinity for ligand. Small molecule integrin antagonists bind with diffusion-limited kinetics (Eg-

[3]Correspondence: springeroffice@cbr.med.harvard.edu

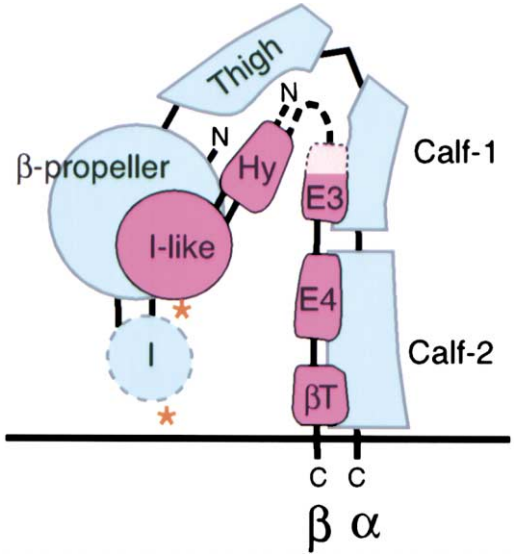

Figure 1. Domain Organization in the Bent Conformation of the αVβ3 Integrin Crystal Structure

Hy, hybrid domain; E3 and E4, integrin EGF domains 3 and 4, respectively; βT, β-tail domain; N, N terminus; C, C terminus. An I domain (I), which is absent in αVβ3, is placed where it is connected in integrins containing I domains. Asterisks mark the position of ligand binding sites at a β propeller-I-like domain interface in integrins that lack I domains, and on the "top" of the I domain in integrins that contain I domains. In β3, the PSI domain at the N terminus and the integrin EGF domains 1 and 2 following the hybrid domain are missing from the electron density, as is a portion of domain 3; these are symbolized with dashed black lines. Polypeptide chain connections are shown as black lines. Note the two polypeptide chain connections between the I-like and hybrid domains in the β subunit, and between the I and β propeller domains in the α subunit. Based on the crystal structure in Xiong et al., 2001.

bertson et al., 1999) and thus must bind to the resting conformation; otherwise, conformational change would limit the on-rate. Furthermore, two-step kinetics suggest that conformational rearrangement, with an increase in overall affinity, occurs subsequent to binding of high affinity ligand-mimetics to integrins (Bednar et al., 1997), as is confirmed by induction of ligand-induced binding site (LIBS) epitopes (Bazzoni and Hemler, 1998; Du et al., 1993; Frelinger et al., 1990; Kouns et al., 1992). Therefore, soaking of ligand into a crystal containing αVβ3 in a low affinity conformation might well lead to visualization of a complex in the low affinity state, with the packing in the crystal lattice preventing conformational rearrangement to the high affinity state that would otherwise occur.

Inside-out signals are thought to activate integrins by breaking a clasp between the α and β subunit cytoplasmic or transmembrane domains (Hughes et al., 1996; Lu et al., 2001b; Takagi et al., 2001; Vinogradova et al., 2002 [this issue of *Cell*]). However, how this could be communicated to the extracellular domains is unclear, just as it is unclear how in the reverse direction, ligand binding to the extracellular domain can be communicated to the cytoplasmic domains. The question is particularly perplexing, since many domains in the α and β subunit legs intervene between the ligand binding headpiece and the membrane, and transmission of conformational change through so many domains is unprecedented. Here, we describe the rearrangements in integrin architecture that communicate signals between the extracellular and intracellular environments, and that regulate affinity for biological ligands.

Results

A Global Shape Change upon Integrin Activation

A soluble extracellular fragment of αVβ3 was made that contained a releasable, C-terminal clasp. The complete extracellular domains of the αV and β3 chains were fused at the C terminus to peptides that formed a disulfide-linked α-helical coiled-coil to mimic the closely positioned and interacting α and β subunit transmembrane helices on the cell surface (Hughes et al., 1996; Lu et al., 2001b; Takagi et al., 2001; Vinogradova et al., 2002 [this issue of *Cell*]). A 13 residue linker between the β subunit and the coiled-coil peptide contained a TEV protease site to enable release of the C-terminal intersubunit clasp by specific cleavage. Because of this linker, the clasp only constrained the C termini of the α and β subunits to be within ~40 Å of one another, and the clasp functions more like a safety catch in a necklace than a clamp. A His C-terminal tag enabled purification under mild conditions. Protein was purified in the presence of 1 mM Ca^{2+} and Mg^{2+}, and half was treated with TEV protease to cleave the clasp. The clasped and unclasped αVβ3 preparations were then further purified by gel filtration in buffer containing either 5 mM Ca^{2+} (a condition resembling the crystallization buffer used by Xiong et al., 2001), 1 mM Mg^{2+}/1 mM Ca^{2+}, or 1 mM Mn^{2+}. Other samples were treated with a high affinity (IC_{50} = 2.5 nM) ligand mimetic peptide (Dechantsreiter et al., 1999), cyclo(Arg-Gly-Asp-D-Phe-Val) (cyclo-RGDfV) in Ca^{2+} or Mn^{2+}, and similarly subjected to gel filtration in the presence of the appropriate divalent cation and cyclo-RGDfV. Negatively stained samples were imaged with an electron microscope (Figure 2, upper portion of each panel). Well resolved particles typical of each treatment were selected and subjected to computational classification and image averaging. Four representative class averages are shown for each treatment (Figure 2, lower portion of each panel).

Whether or not the clasp was cleaved, the αVβ3 images obtained in the presence of 5 mM Ca^{2+} (Figures 2A and 2B) and 1 mM Mg^{2+}/1 mM Ca^{2+} (data not shown) looked very similar, with the majority of the particles assuming a compact V-shaped conformation. In the presence of Ca^{2+} and the C-terminal clasp, the molecules were overwhelmingly (~95%) compact, and had the V-shaped appearance distinctive of the bent conformation of αVβ3 seen in the crystal structure (Figure 2A, averages 1, 2, and 4). The majority (~86%) of the TEV protease-treated, unclasped αVβ3 molecules in the presence of Ca^{2+} also showed a compact structure (Figure 2B). However, a lesser fraction of about 55% of the compact molecules adopted the same V-shaped conformation as clasped αVβ3 (Figure 2B, averages 1 and 2), whereas the other molecules were somewhat less compact (Figure 2B, averages 3 and 4). The remaining ~5% and ~14% of the clasped and unclasped particles, respectively, had an extended conformation

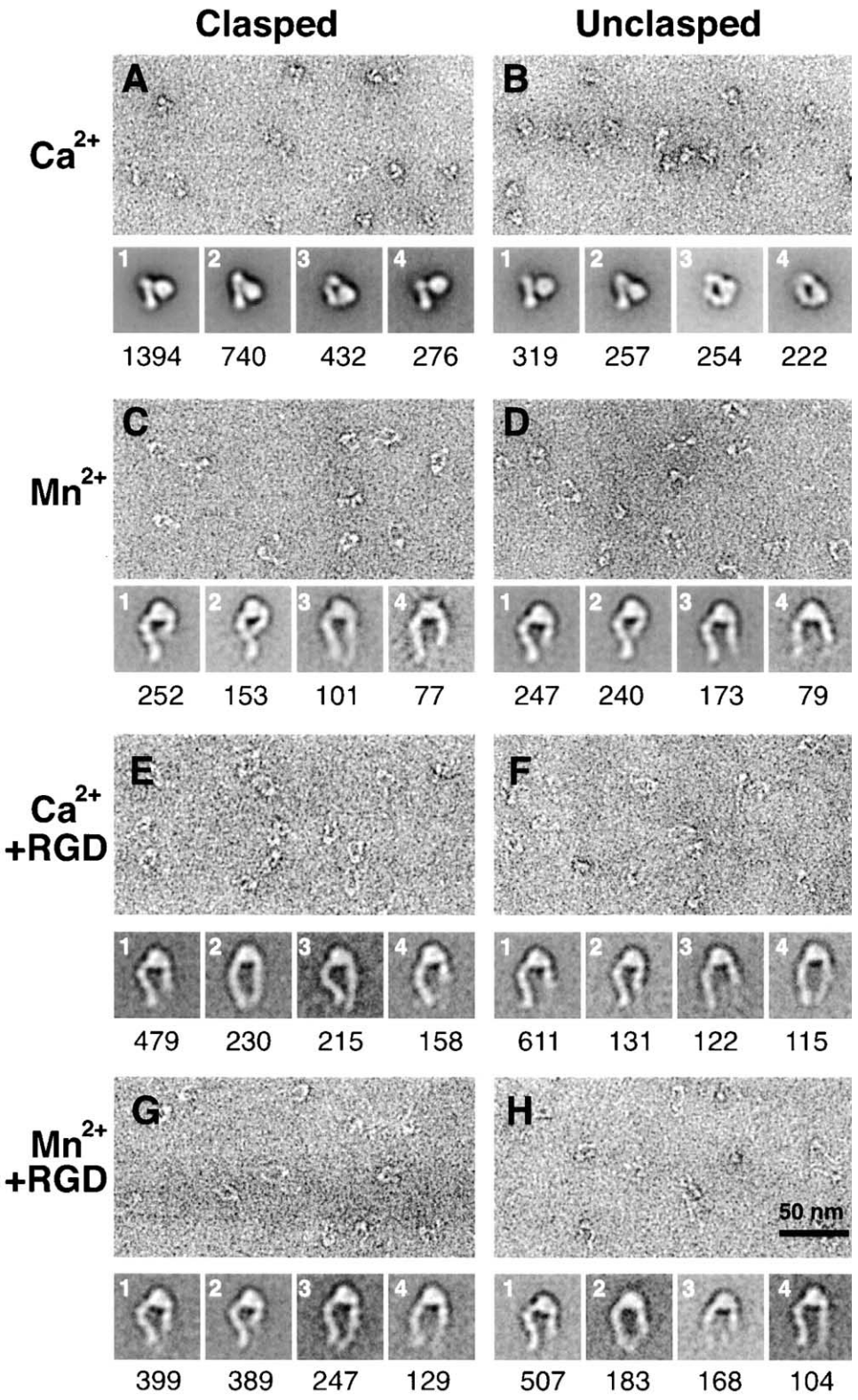

Figure 2. Electron Micrographs and Representative Projection Averages of Negatively Stained αVβ3 Integrin

Clasped αVβ3 (A, C, E, and G) and unclasped αVβ3 (B, D, F, and H) were incubated in the presence of 5 mM Ca^{2+} (A and B), 1 mM Mn^{2+} (C and D), 1 mM Ca^{2+} and 60 μM cyclo-RGDfV peptide (E and F), or 1 mM Mn^{2+} and 60 μM cyclo-RGDfV (G and H) and subjected to gel filtration, negative staining, and electron microscopy. Each panel shows a micrograph area as well as four representative projection averages. The number of individual particles represented by each projection average is shown beneath each average, and reflects the relative frequency among all particles used in averaging. The minority of extended particles in (A) and (B) were not chosen for averaging; their percentage of the total particles is described in the text; similarly, compact particles were not chosen for averaging in (C)–(H) and their percentage is given in the text. The side length of the average images is 28.4 nm.

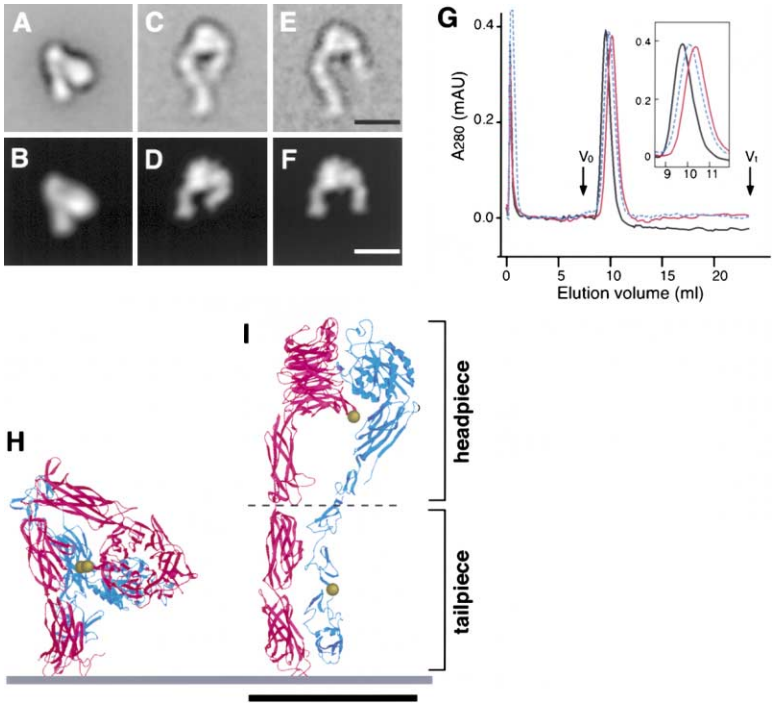

Figure 3. Comparison of Negatively Stained αVβ3 Projection Averages to the αVβ3 Crystal Structure and Hydrodynamic Properties

(A) Projection average of clasped αVβ3 particles in the presence of Ca^{2+} used for cross-correlation in (B). (B) Best correlating projected view calculated from the αVβ3 crystal structure (Xiong et al., 2001). (C) Representative projection average of an extended integrin with a closed headpiece (unclasped in Mn^{2+} from Figure 2D, average 2) used in cross-correlation. (D) Best correlating projected view calculated from the headpiece of the αVβ3 crystal structure (1JV2); the corresponding headpiece from the ligand-complexed structure (1L5G) gave an identical cross-correlation rotation function and projected view. (E) Representative projection average of an extended integrin with an open headpiece (unclasped in Ca^{2+} + cyclo-RGDfV, from Figure 2F, average 1) used in cross-correlation. (F) Best correlating projected view calculated from the model of the open headpiece crystal structure. The model was made from the αVβ3 crystal structure (1JV2) by superimposing β3 residues D109, A347 and Y348 on residues D109, I351, and R352 to simulate a 4 residue downward shift of the I-like domain C-terminal α helix. Hybrid domain residues 55–109 and 348–434 from the superimposed structure were combined with the remaining headpiece residues from the 1JV2 structure to make the open model. The bar indicates 100 Å. (G) Change in hydrodynamics of αVβ3 induced by Mn^{2+} or ligand binding. Unclasped αVβ3 (1.8 μg in 10 μl) was analyzed on a Superdex 200 column in a buffer containing 1 mM Ca^{2+} (red line), 1 mM Mn^{2+} (blue dotted line), or 1 mM Mn^{2+} + 1 μM cyclo-RGDfV (black line). Arrows indicate excluded volume (V_0) and total volume (V_t) of the column. A rescaled view of the peak position is shown in the inset. (H and I) Ribbon diagrams of the alternative conformations of the extracellular segment of αVβ3 integrin. The bent conformation observed in the crystal structure (1JV2) with I-EGF domains 1, 2, and a portion of 3 built in similar to the model described in (Beglova et al., 2002) is shown in (H), and a corresponding model of the extended conformation is shown in (I). The model of the unbent molecule was created by breaking the bent form at the junction between the thigh and calf-1 domains in α and I-EGF1 and 2 in β (dashed line) into the headpiece and tailpiece, and moving the headpiece relative to the tailpiece. The approximate position of the cell membrane is indicated by a gray line. Black bar indicates 100 Å.

(not shown). The percentage of compact versus extended particles and the percentage of compact particles with the V-shaped conformation suggest that the clasp between the C-terminal tails of the αV and β3 subunits favors the compact, V-shaped conformation.

The compact, V-shaped structure of αVβ3 particles in Ca^{2+} is highly similar to the bent conformation seen in αVβ3 crystals (Xiong et al., 2001). To verify these similarities, the atomic coordinates from the crystal structure were used to calculate evenly spaced 2D projections, which were then compared to our projection map by cross-correlation (Frank et al., 1996). This procedure identified a projection of the crystal structure (Figure 3B) that was in excellent agreement with our EM projection average (Figure 3A). One leg of the V ends in a large globule corresponding to the integrin headpiece, while the other leg corresponds to the tailpiece. The tip of the V corresponds to the genu. In the headpiece, the β propeller domain is oriented in the cross-correlated crystal structure with the pseudosymmetry axis in the

Table 1. Gel Filtration Behavior of αVβ3 Integrin in Various Conditions

Condition	Elution volume[a] (ml)	Stokes radius[b] (nm)
Clasped αVβ3		
Ca^{2+}, no ligand	10.50 ± 0.03	5.58
Ca^{2+}, +RGDfV	9.81 ± 0.02	6.36
Mn^{2+}, no ligand	10.29 ± 0.03	5.81
Mn^{2+}, +RGDfV	9.80 ± 0.04	6.37
Unclasped αVβ3		
Ca^{2+}, no ligand	10.34 ± 0.03	5.75
Ca^{2+}, +RGDfV	9.79 ± 0.02	6.39
Mn^{2+}, no ligand	10.10 ± 0.02	6.02
Mn^{2+}, +RGDfV	9.77 ± 0.04	6.42

[a] Mean ± SD (n = 3 for clasped and 4 for unclasped αVβ3).

[b] Calculated from the elution positions of standard proteins with known Stokes radius values: 8.5 nm for thyroglobulin, 6.1 nm for apoferritin, 3.55 nm for serum albumin, and 1.70 nm for cytochrome c. **: $p < 0.001$, *: $p < 0.01$ by Student's t test.

central cavity normal to the grid; remarkably, the central cavity is evident in some of the EM projection averages (Figure 2A, averages 1 and 4; Figure 2B, averages 1 and 2). The angles between the legs of the V in the crystal structure and the predominant EM projections are the same, showing that the degree of bending is not a crystal structure artifact but occurs in individual unconstrained molecules as well. The crystal structure thus represents the predominant native conformation of αVβ3 in the presence of Ca^{2+} or Ca^{2+}/Mg^{2+}. An average representing a small fraction (10%) of the closed particles has a somewhat wider angle between the tailpiece and headpiece (Figure 2A, average 4). Therefore, some breathing between the headpiece and tailpiece may occur.

Mn^{2+} activates all integrins, apparently by binding to the MIDAS of the I-like domain (Shimaoka et al., 2002). Although it binds to the extracellular segment of integrins, Mn^{2+} appears in many respects to mimic inside-out signaling, both by activating in the absence of a bound ligand, and in exposing a similar array of activation epitopes. In the presence of Mn^{2+}, a fraction of the αVβ3 molecules (~15% and ~20% for clasped and unclasped αVβ3, respectively) remained in the compact conformation (not shown); however, the vast majority underwent a dramatic, global change in conformation and converted to an extended form (Figures 2C and 2D), with a globular head connected to two long legs. This shape resembles that seen previously in EM studies on integrins (Du et al., 1993; Nermut et al., 1988; Takagi et al., 2001).

Binding by ligand-mimetic peptides to integrins mimics signaling from the ligand binding site to the membrane proximal segments of the α and β subunits. Incubation with cyclo-RGDfV in the presence of Ca^{2+} (Figures 2E and 2F) or Mn^{2+} (Figures 2G and 2H) induced an extended conformation of αVβ3 similar to that seen in Mn^{2+}; however, in contrast to Mn^{2+} alone, conversion to the extended conformation was essentially complete: more than 98% of the molecules were fully extended. Importantly, the αVβ3-RGDfV complex adopted a fully extended conformation even in the presence of Ca^{2+}, indicating that ligand binding results in the global conformational rearrangement of the integrin molecule.

Complementary measurements of shape change in solution were made on the same integrin preparations using analytical gel filtration. The hydrodynamic Stokes radius of 5.6 to 5.7 nm of clasped and unclasped αVβ3 was increased by cyclo-RGDfV in Ca^{2+} or Mn^{2+} to 6.4 nm (Figure 3G) (Table 1). The Stokes equation calculates the size of a hard sphere with an equivalent frictional coefficient; however, the increase in hydrodynamic radius of αVβ3 when complexed with cyclo-RGDfV must actually be due to an increase in asymmetry, which may be expressed as an axial ratio (*a*/*b*) (Tanford, 1961). The observed increase corresponds to a 2- to 3-fold increase in the axial ratio, which agrees well with the approximate doubling in length that occurs when the V-shaped integrin in Ca^{2+} is converted by cyclo-RGDfV to the fully extended molecule.

Treatment with Mn^{2+} alone resulted in a hydrodynamic radius for αVβ3 intermediate between that in Ca^{2+} alone and in complex with cyclo-RGDfV (Table 1). This agreed with EM measurements showing that both compact αVβ3 and extended αVβ3 were present in Mn^{2+}, whereas in Ca^{2+} only compact αVβ3 was present, and in cyclo-RGDfV only extended αVβ3 was present. Interestingly, the elution peaks for all treatments showed a single, sharp, symmetric peak (Figure 3G), despite the observation by EM of two shapes in Mn^{2+}. This shows that the compact and extended structures must be in rapid equilibrium, with interconversion occurring on a timescale much more rapid than the time for elution from the gel filtration column of ~13 min. Furthermore, the hydrodynamic radius in Mn^{2+} did not increase with time. Whether unclasped samples were subjected to gel filtration immediately after addition of Mn^{2+} or 135 min later, the elution position was the same.

Structural Details of the Extended Integrin Conformation

In the EM images, the side of the headpiece containing the α subunit is distinguished by the thicker coating of negative stain outlining the α subunit/β-propeller domain (Figures 2C–2H), a consequence of this large domain extending further above the carbon film. Integrin heterodimers containing a full-length α subunit and a β subunit truncated after the hybrid domain confirmed this sidedness (J.T., T.A.S., and T.W., unpublished results). In Figures 2C–2H, all averaged images are shown with the headpiece toward the top of the page and the α subunit on the left. In all conditions giving extended structures, the α subunit leg appears in a relatively uniform orientation (Figures 2C–2H). This suggests that after unbending at the genu between the thigh and calf-1 domains (Xiong et al., 2001), the interface between these domains snaps into a relatively uniform orientation in the extended conformation. The uniform orientation of the αV leg also suggests that the interfaces between the β propeller and thigh domains, and between the calf-1 and calf-2 domains, are in a relatively fixed orientation. The angles between these domains are similar to those observed in the crystal structure (Xiong et al., 2001). Three centers of density along the αV leg may correspond to the thigh, calf-1, and calf-2 domains.

Most averaged images showed only about the upper half of the β leg. The upper β leg usually contained one density near the headpiece corresponding to the hybrid domain (see below, Figure 3C). A second more distal density was also sometimes present (e.g., Figure 2D average 4; Figure 2F average 2), which may correspond to the PSI domain and integrin EGF domain 1, which are disordered in the crystal structure. Because the lower leg varied in conformation among individual particles, averaging tended to make it disappear. However, some averages particularly of clasped αVβ3 showed the complete β leg (Figure 2C average 3; Figure 2E average 3; Figure 2G average 3), which appears longer than the α leg.

The upper portion of the β3 leg differs in the angle it makes with the headpiece among different classes of averaged projections. In Mn^{2+} and absence of cyclo-RGDfV, an acute angle is seen in some averages (Figure 2C, averages 1 and 2; Figure 2D, average 2) and a more obtuse angle in others (Figure 2C, averages 3 and 4; Figure 2D, averages 1, 3, and 4). We refer to these as the closed and open conformations of the headpiece, respectively. In Mn^{2+} alone, a higher proportion of un-

clasped particles (~70%) had open headpieces than clasped particles (~30%). Binding to cyclo-RGDfV in Ca^{2+} or Mn^{2+} resulted in uniform adoption of the open conformation of the headpiece, with all averages showing wide separation between the α and β legs near the headpiece (Figures 2E–2H).

The images of the extended conformation were compared to the αVβ3 crystal structures. The crystal structure coordinates were truncated at the positions of the bends in αV and β3 (Figure 1) to obtain the fragment corresponding to the headpiece, and cross-correlated to representative EM projection averages in which the β leg was in the acute (closed) or obtuse (open) orientation to the headpiece (Figures 3C and 3E, respectively). Cross-correlation confirmed that in the orientation shown (Figures 3C and 3E), the α subunit/β propeller, and β subunit I-like domains combine to form the globular head, and the α thigh and β hybrid domains project from the bottom of the globule on the left and right, respectively. Therefore, the hybrid domain has two different orientations relative to the I-like domain. The crystal structures (Figure 3D) match the closed orientation found in averages in Mn^{2+} (Figure 3C), but clearly do not match the open orientation seen in averages in Mn^{2+} and in all the averages in which cyclo-RGDfV is bound in Ca^{2+} or Mn^{2+} (Figure 3E). Thus, a conformational change occurs upon activation by Mn^{2+} or cyclo-RGDfV that changes the orientation of the I-like domain relative to the hybrid domain.

Integrin I domains are activated by a downward movement of the C-terminal α helix (Shimaoka et al., 2002). Modeling the effect of a one turn (four residue) downward movement of the C-terminal α helix of the I-like domain shows that it causes the hybrid domain to pivot about its connection to the N terminus of the I-like domain, and swing away from the α thigh domain and make the headpiece more open (Figure 3F). The cross-correlation coefficient of the open EM images in cyclo-RGDfV (Figure 3E) with the open headpiece model (Figure 3F) was 893, significantly better than the coefficients of 729 and 730 obtained with the headpieces from the uncomplexed and peptide-complexed crystal structures (Figure 3D), respectively.

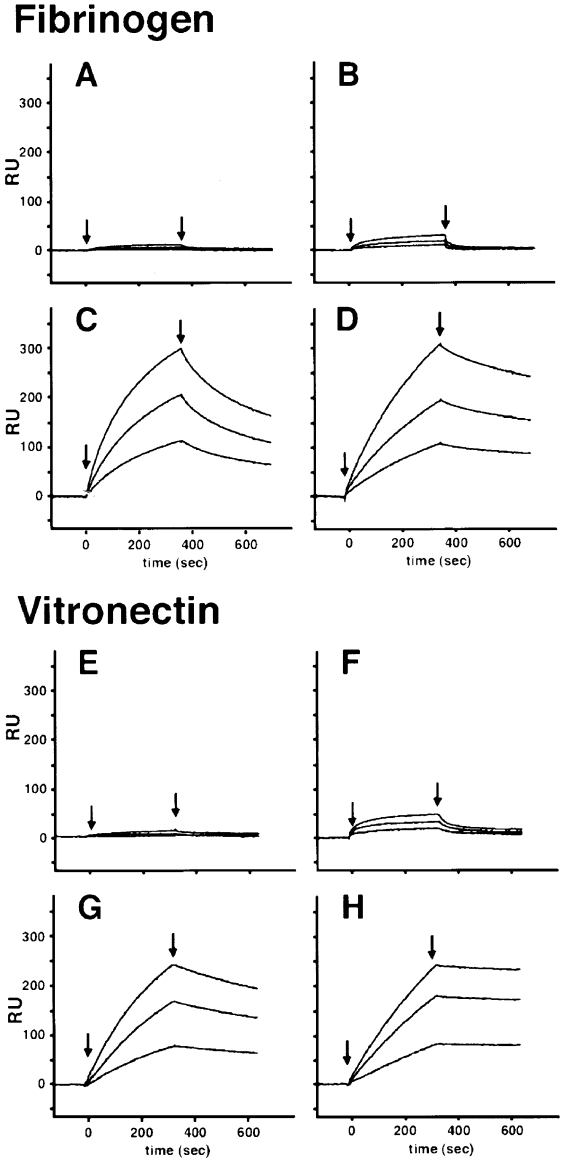

Figure 4. Activation by Mn^{2+} of Ligand Binding by αVβ3

Surface plasmon resonance shows specific binding of clasped (A, C, E, and G) or unclasped (B, D, F, and H) αVβ3 in the presence of 1 mM Ca^{2+}/1 mM Mg^{2+} (A, B, E, and F) or 1 mM Mn^{2+} (C, D, G, and H) to the sensor chip coated with human fibrinogen (A–D) or human native vitronectin (E–H). The traces show increasing concentrations (50, 100, and 150 nM) of αVβ3 analyte. Arrows indicate start and end points of the injection.

The Extended but Not the Bent Conformation Has High Affinity for Biological Ligands

Binding of the biological ligands fibrinogen or vitronectin was measured in solution phase using surface plasmon resonance and the same αVβ3 preparations as used in EM and gel filtration studies. In the presence of physiological divalent cation concentrations of 1 mM Ca^{2+} and 1 mM Mg^{2+}, little or no binding of fibrinogen or vitronectin to clasped αVβ3 was observed (Figures 4A and 4E), and release of the C-terminal clasp only slightly increased binding (Figures 4B and 4F). By contrast, when the binding was measured in a buffer containing 1 mM Mn^{2+}, concentration-dependent binding to the immobilized fibrinogen as well as vitronectin was observed with both clasped and unclasped αVβ3 (Figures 4C, 4D, 4G, and 4H). The curves fit well to a 2-step binding model, but not a 1-step Langmuir binding model. These findings suggest two steps: (1) ligand binding, and (2) rearrangement to a conformation in which ligand is bound with higher affinity, as has previously been reported for αIIβ3 binding to fibrinogen and high-affinity RGD mimetics (Bednar et al., 1997; Huber et al., 1995). Therefore, for simplicity we report here apparent association and dissociation rate constants derived from the initial phase of the association and dissociation curves, respectively. The k_{on} values are similar for clasped and unclasped αVβ3 in Mn^{2+}: $5.1 \times 10^4\ M^{-1}\ s^{-1}$ for fibrinogen and $7.9 \times 10^3\ M^{-1}\ s^{-1}$ for vitronectin. These are comparable to the k_{on} values of $2.5 \times 10^4\ M^{-1}\ s^{-1}$ for fibrinogen and $2.3 \times 10^3\ M^{-1}\ s^{-1}$ for vitronectin reported for detergent-solubilized αVβ3 in a solid phase binding assay in the presence of

Mn^{2+} (Smith et al., 1994). Ligand dissociated more slowly from unclasped than clasped αVβ3. The initial rate of dissociation from fibrinogen was 9.8×10^{-4} and 2.8×10^{-3} s^{-1} for unclasped and clasped αVβ3, respectively. Similarly, the rate of dissociation from vitronectin was 2.1×10^{-4} and 9.2×10^{-4} s^{-1} respectively. Therefore, release of the C-terminal intersubunit constraint, which mimics uncoupling of the transmembrane/cytoplasmic domain interaction between the α and β subunits, results in stronger association with ligand. The combined structural and binding studies show that the bent conformation of αVβ3 in the presence of Ca^{2+} and Mg^{2+} has little affinity for ligand, whereas the extended conformation in the presence of Mn^{2+} has high affinity for ligand.

We used mutational introduction of disulfide bonds to confirm that cell surface integrins also assume the bent conformation, and that they are inactive in this bent conformation. In the extended conformation of αVβ3, Gly-307 in the β-propeller domain of αV and Arg-563 in I-EGF domain 4 of β3 are far apart (Figure 3I, gold spheres). In the bent conformation of the αVβ3 crystal structure, however, the Cα atoms of these two residues are only 5.2 Å apart (Figure 3H, gold spheres). Since this distance is compatible with disulfide bond formation between cysteines, Gly-307 of αV (or the corresponding residue in αIIb, Arg-320) and Arg-563 of β3 were mutated to cysteine residues to test inter-subunit disulfide bridge formation. Lysates from ^{35}S-labeled 293 T cell transfectants were subjected to immunoprecipitation and nonreducing SDS-PAGE (Figure 5A). Remarkably, when mutant αV or αIIb subunits were cotransfected with the mutant β3 subunit, covalently linked heterodimers were formed (Figure 5A, lanes 2 and 6). By contrast, cotransfection of mutant α with wild-type β (Figure 5A, lanes 3 and 7) or wild-type α with mutant β (Figure 5A, lanes 4 and 8) resulted in migration of the α and β subunits as monomers, as observed for the wild-type α and β combination (Figure 5A, lanes 1 and 5). When the samples were reduced prior to electrophoresis, all α and β species migrated as monomers (data not shown). The close proximity of residue 307 of αV to residue 563 of β3 in cell surface αVβ3, and of residue 320 of αIIb to residue 563 of β3 in cell surface αIIβ3 as demonstrated by disulfide bond formation, shows that integrin heterodimers can indeed adopt the bent conformation on the cell surface.

We tested the effect on ligand binding of locking the bent conformation into cell surface integrins with a disulfide bond. Since binding of soluble ligands to β3 integrins is strictly dependent on high-affinity receptors (Pampori et al., 1999), we looked at the binding of fluorescently labeled fibrinogen to cells expressing either wild-type or mutant αVβ3 and αIIbβ3. Wild-type αVβ3 or αIIbβ3 expressed in 293T cells did not bind FITC-fibrinogen under basal conditions in Ca^{2+}, but bound well after activation with Mn^{2+} and activating mAbs (Figure 5B). By contrast, cells expressing αVβ3 and αIIbβ3 with cysteine mutations in both α and β subunits were resistant to activation, as shown by a lack of ligand binding after stimulation with Mn^{2+} and activating mAb (Figure 5B). Despite its activating effect on some assays of integrin function (Yan and Smith, 2001), reduction with dithiothreitol (DTT) did not affect fibrinogen binding by wild-type transfectants (Figure 5B), presumably because high affinity is required for binding of the soluble ligand. By contrast, reduction with DTT enabled cells bearing αVβ3 and αIIbβ3 integrins with the cysteine mutations to bind FITC-fibrinogen in response to activating agents (Figure 5B). These results demonstrate that a disulfide bridge between headpiece and tailpiece residues locked two different β3 integrins in a conformation incompetent for high-affinity ligand binding. Inhibition of ligand binding, and demonstration of disulfide bond formation, was similarly obtained when we introduced cysteines into β3 residues 332 in the I-like domain and 674 in the β-tail domain to stabilize the bent conformation (data not shown).

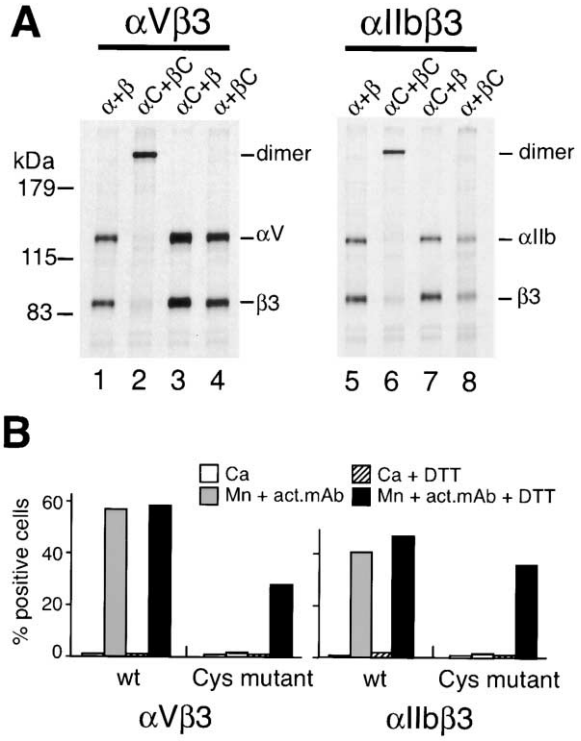

Figure 5. Cell Surface αVβ3 and αIIbβ3 Kept in the Bent Conformation Is Locked in an Inactive State

(A) Disulfide bond formation between the headpiece of the α subunit and tailpiece of the β subunit. 293T cells were cotransfected with wild-type (α and β) or mutant (αC and βC) integrin subunits to give the indicated α/β pairs. αC denotes αV^{G307C} or αIIb^{R320C}, βC denotes $\beta 3^{R563C}$. Integrin heterodimers were immunoprecipitated from the ^{35}S-labeled cell extract with AP3 mAb to β3 and subjected to nonreducing SDS-PAGE and fluorography. Positions for molecular size markers are shown on the left. (B) Binding of fibrinogen to β3 integrins. The conversion to the high-affinity state was assessed by binding of FITC-fibrinogen to αVβ3 or αIIbβ3 using fluorescence flow cytometry. 293T cell transfectants expressing wild-type or double cysteine mutants ($\alpha V^{G307C}\beta 3^{R563C}$ or $\alpha IIb^{R320C}\beta 3^{R563C}$) were treated with 5 mM Ca^{2+} or 1 mM Mn^{2+} plus activating mAbs (AP5 for αVβ3, PT25-2 for αIIbβ3), with or without 2 mM DTT and incubated with 30 μg/ml of FITC-fibrinogen for 30 min at room temperature. Data are representative of three independent experiments.

Discussion

Three Integrin Conformational States

We have demonstrated that integrins exist in at least three conformational states: a bent conformer (Figure

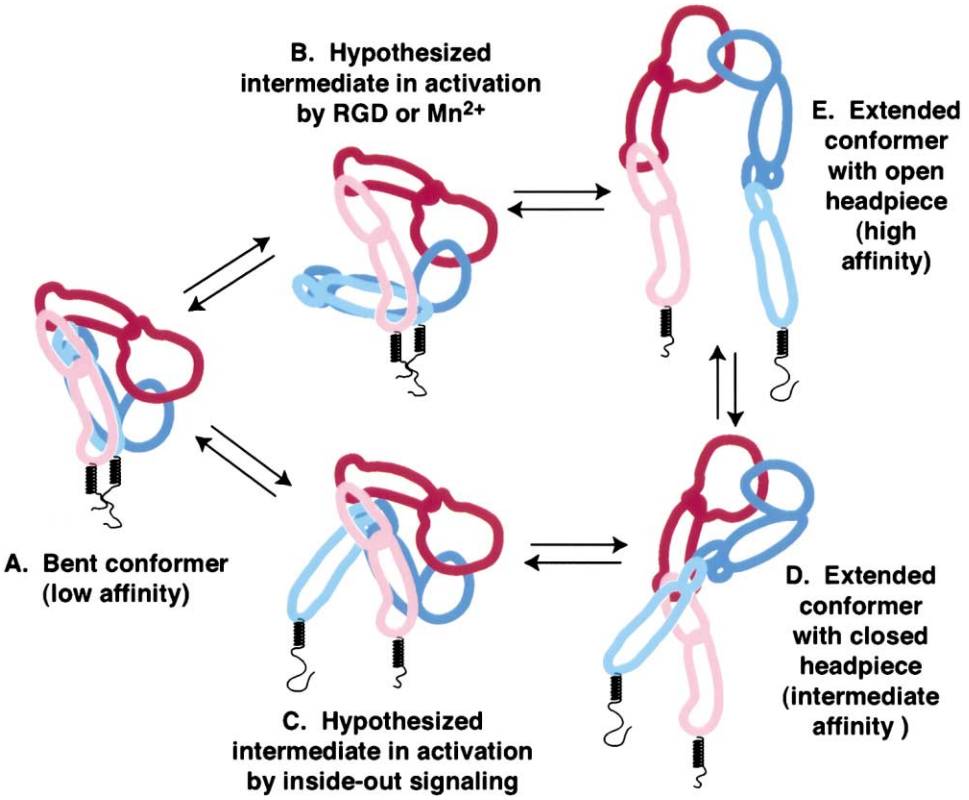

Figure 6. Quaternary Structural Rearrangements in Integrin Activation

The three conformers defined by electron microscopy (A, D, and E) and the hypothetical intermediates when the headpiece-tailpiece and α tailpiece-β tailpiece interfaces are destabilized in outside-in (B) or inside-out (C) signaling are schematized. The α headpiece domains (β-propeller and thigh) are red, α tailpiece domains (calf-1 and calf-2) are pink, β headpiece domains (I-like, hybrid, PSI, and I-EGF1) are blue, and β tailpiece domains (I-EGF2, and the I-EGF3, I-EGF4, and β-tail which are shown merged together) are cyan. Black squiggly lines symbolize the transmembrane and cytoplasmic domains. The conformers are shown in the same orientation as the cross-correlated headpiece in Figure 3C, except for rotation in the plane of the figure. The rotation in the plane of the figure is such as to maximize comparison between the conformers, and is not uniform with regard to expected orientation relative to the cell membrane, especially in (D).

6A), an extended conformer with a closed headpiece (Figure 6D), and an extended conformer with an open headpiece (Figure 6E). Our studies unequivocally establish that the bent conformation exists in solution and on cell surfaces, and represents the highly physiologically relevant low-affinity conformation of integrins. The bent conformer is seen in Ca^{2+}/Mg^{2+} and Ca^{2+}, is stabilized by Ca^{2+}, strongly destabilized by cyclo-RGDfV, and less strongly destabilized by Mn^{2+}. In the presence of a C-terminal clasp, a higher proportion of αVβ3 molecules is present in the V-shaped bent conformation in Ca^{2+}. The bent αVβ3 conformer does not bind the biological ligands fibrinogen or vitronectin as shown in solution phase binding assays in Ca^{2+}/Mg^{2+}. On the cell surface, αVβ3 and αIIbβ3 cannot be stimulated to bind their biological ligand fibrinogen with high affinity when locked in the bent conformation with a disulfide bond. Activation of ligand binding by the locked bent integrins, but not by wild-type integrins, requires disulfide reduction. Although the bent conformer does not detectably bind biological ligands, it clearly can bind high-affinity ligand-mimetic peptides as demonstrated by a co-crystal structure (Xiong et al., 2002). We therefore refer to the bent conformer as a low-affinity rather than an inactive conformation.

In Mn^{2+}, the bent conformer and the two extended conformers with the open and closed headpiece were all present as shown with EM. Physiochemical measurements demonstrated a conformational equilibrium in Mn^{2+}, with equilibration between the bent and extended conformers occurring on a timescale much more rapid than 13 min. In Mn^{2+}, αVβ3 bound to fibrinogen and vitronectin, demonstrating that one or both of the extended conformers has high affinity for ligand. A higher percentage of molecules in the extended conformation were found for unclasped than clasped αVβ3 in Mn^{2+}, correlating with the finding that unclasped αVβ3 has higher affinity for vitronectin and fibrinogen.

In the presence of cyclo-RGDfV, the equilibrium shifted almost entirely to the extended conformer of αVβ3 with the open headpiece. The same results were seen in Ca^{2+} or Mn^{2+} and with clasped or unclasped αVβ3. Cyclo-RGDfV was used at concentrations far above its K_D, which will drive the conformational equilibrium to the conformer with the highest affinity for ligand. This identifies the extended conformer with the open headpiece as the conformation with highest affinity for ligand (Figure 6E).

The extended conformer with the closed headpiece (Figure 6D) represents an intermediate conformation,

because it shares the closed headpiece with the bent conformer, and shares the lack of a tailpiece-headpiece interface with the extended conformer with the open headpiece. The presence of all three species of conformers in Mn^{2+}, and only the bent conformer in Ca^{2+} alone and only the extended, open conformer in cyclo-RGDfV also suggests that the extended, closed conformer is an intermediate in the conformational equilibrium between the low and high affinity forms. Because the equilbria of conformational change and ligand binding are thermodynamically linked (Marvin and Hellinga, 2001), it is reasonable to assume that the extended, closed conformer has an intermediate affinity for ligand (Figure 6D).

Integrins vary markedly in their susceptibility to activation, e.g., as demonstrated among different β1 integrins in ability of Mn^{2+} or soluble ligands to induce expression of β1 subunit activation epitopes (Bazzoni et al., 1998). Electron microscopy of clasped α5β1 and αIIbβ3 integrins prepared similarly to clasped αVβ3 shows that in Ca^{2+} they also adopt the bent conformation (data not shown). However, a significantly higher proportion of particles adopted the extended conformation in Ca^{2+} than seen with αVβ3. Therefore, the equilibrium point between the bent and extended conformations may differ depending on the integrin. It may be more appropriate to think of activators or inhibitors as influencing the equilibria that relate conformers, rather than locking in a particular conformation. Almost all factors with which integrins interact, such as cytoplasmic proteins (Liu et al., 2000) and the TM4 superfamily proteins (Hemler, 1998), may influence the conformational equilibria.

The Switchblade Model of Integrin Activation

We have shown that activation of αVβ3 with Mn^{2+} or cyclo-RGDfV results in a dramatic rearrangement of the quaternary structure to an extended conformation. Previous electron micrographic studies of native or recombinant integrins have generally visualized the extended conformation (Du et al., 1993; Nermut et al., 1988; Takagi et al., 2001). Although in some cases compact globules were also reported, they may have largely escaped notice because (1) integrins such as αIIbβ3 and α5β1 are less stable in the bent conformation than αVβ3, (2) harsh elution conditions activate integrins and induce the extended conformation, and (3) all previous studies utilized the lower resolution technique of rotary shadowing, in which the bent conformation appears as a globule and lacks interesting fine structure.

Many anti-integrin mAbs have been reported that bind preferentially to the active and/or ligand-occupied form of integrins (Bazzoni and Hemler, 1998; Shimaoka et al., 2002). Recently, a combined NMR structure and model of β2 integrin I-EGF modules 2 and 3 (Beglova et al., 2002) localized epitopes of mAb that report integrin activation and induce integrin activation (Lu et al., 2001a), and residues that interact with the α subunit to restrain activation (Zang and Springer, 2001). These residues are buried in the bent conformation, but exposed in an extended conformation. Therefore, we postulated a switchblade-like opening of the bent conformation upon integrin activation (Beglova et al., 2002). The studies presented here confirm and markedly extend the switchblade model. The identification of the bent αVβ3 conformer as the low affinity, resting state of integrins on the cell surface, and the shift of the conformational equilibrium toward the extended conformer by activation and ligand binding explain many previous results on LIBS and activation-dependent epitopes, including the presence of the vast majority of these epitopes on the β subunit. In the bent αVβ3 structure, the β subunit is innermost in the bend (Figure 3H) and contributes about 70% of the solvent accessible surface area that is buried in the headpiece-tailpiece interface (Table 2). A minority of αVβ3 particles in Ca^{2+} had a V-shaped conformation with a wider separation between the headpiece and tailpiece. This provides direct evidence for "breathing" at this interface, as previously hypothesized (Beglova et al., 2002). Upon temporary exposure of the headpiece-tailpiece interface during breathing movements, binding of an antibody to the inner side of the β tail would keep the interface wedged open, prevent rebending of the receptor, and stabilize the extended conformation and hence ligand binding. It is interesting that antibodies that map further from the bend can bind to resting integrins and activate them, whereas a mAb that binds only after prior integrin activation binds close to the bend, where less opening would occur during breathing (Beglova et al., 2002).

Table 2. Solvent Accessible Surface Area Buried in Tailpiece-Headpiece and α Tailpiece-β Tailpiece Interfaces in αVβ3[a]

	Headpiece-tailpiece	α tailpiece-β tailpiece	α headpiece-β headpiece
Domain	Solvent accessible surface area buried (Å²)		
α β-propeller	260	-	1640
α thigh	250	-	-
α calf-1	290	400	-
α calf-2	0	730	-
β hybrid	630	-	50
β I-like	80	-	1720
β I-EGF3	260	250	-
β I-EGF4	260	340	-
β β-tail	360	340	-
Total	2370	2050	3410

[a] The αVβ3 crystal structure (1JV2) (Xiong et al., 2001) was extended by moving the headpiece (α 1-594, β 55-434) relative to the tailpiece (α 595-956, β 532-690) so that the covalent connection between residues 594 and 595 at the genu was maintained and the thigh-calf-1 interface was minimized. The areaimol function of the CCP4 suite was used to compare solvent accessible surface areas of the extended and bent structures (Bailey, 1994). For the α tailpiece-β tailpiece and α headpiece-β headpiece interfaces, the individual α or β subunit segments were placed in separate pdb files and compared to the file containing both segments.

Extracellular Domain Rearrangements in Outside-In Signaling

The structural rearrangements demonstrated here after binding of cyclo-RGDfV to αVβ3 define a pathway for communication from the ligand binding site in the headpiece to the membrane proximal segments of the α and β legs; i.e., the extracellular portion of the integrin outside-in signaling pathway. The cyclo-RGDfV peptide differs only 4-fold in IC_{50} and in one methyl group from its

N-methyl-Val derivative, cyclo-RGDf-mV (Dechantsreiter et al., 1999), which was used in αVβ3 co-crystals (Xiong et al., 2002). When soaked into αVβ3 crystals along with Mn^{2+}, cyclo-RGDf-mV bound to the bent conformation of αVβ3, with its Asp sidechain coordinating the Mn^{2+} in the MIDAS of the β3 I-like domain. By contrast, binding to αVβ3 in solution results in a dramatic quaternary rearrangement to an extended conformation with an open headpiece. The lack of major rearrangements in the crystal structure is readily explained by the extensive lattice contacts stabilizing the bent conformation. Thus, in a first step, peptide binds to the low affinity, bent αVβ3 conformer, which has a closed headpiece; and in a second step, in the absence of crystal lattice constraints, binding causes a dramatic quaternary rearrangement to the high affinity, extended conformer with an open headpiece.

The ligand-induced conformational change directly observed here is consistent with many long-standing observations in the integrin literature which indirectly suggest conformational change: (1) The exposure by biological ligands and by peptidomimetic integrin antagonists of LIBS epitopes far from the ligand binding site itself (Bazzoni and Hemler, 1998; Frelinger et al., 1990; Kouns et al., 1992). (2) Binding of RGD peptides to αIIb β3, followed by washout of the peptide, activates binding of αIIbβ3 in solution and on platelets to fibrinogen (Du et al., 1991). In a related phenomenon, cyclo-RGDfV can augment binding of αVβ3 to fibrinogen, fibronectin, and vitronectin when used near its IC_{50}, but is inhibitory at high concentrations (Legler et al., 2001). (3) Binding of small molecule antagonists and fibrinogen shows two-step binding kinetics (Bednar et al., 1997; Huber et al., 1995), suggesting that after ligand binding, a rearrangement occurs to a conformation with higher affinity for ligand. (4) Conformational change in αIIbβ3 upon binding to small peptide ligands, with a decrease in sedimentation coefficient and an increase in Stokes radius, was noted long ago (Parise et al., 1987).

Both peptidomimetic and antibody antagonists of αIIb β3 are in wide use clinically for treatment of heart disease (Coller, 2001; Scarborough and Gretler, 2000). Both classes of antagonists induce conformational change in αIIbβ3 on the surface of circulating platelets, as well documented with LIBS monoclonal antibodies (Kouns et al., 1992; Peter et al., 1998). This has important clinical implications, because a small subset of patients have pre-existing LIBS antibodies that result in thrombocytopenia (Billheimer et al., 2002; Scarborough and Gretler, 2000). Our direct demonstration here of conformational rearrangements in αVβ3 shows that the possibility of similar reactions must be considered with the αVβ3 antagonists currently undergoing clinical development for treatment of cancer and bone resorption disorders (Brooks et al., 1994; Dechantsreiter et al., 1999).

Our demonstration that integrins adopt a bent conformation in the low-affinity state suggests that a new class of small molecule antagonists to integrins should be sought. Small molecules that bind to and stabilize the headpiece-tailpiece or α tailpiece-β tailpiece interfaces would antagonize integrin activation, and would not act as partial agonists or induce conformational changes that expose LIBS. Analogous inhibitors have been found to αLβ2, that bind to the I domain at a site distal from the ligand binding site, and act by stabilizing the low affinity conformation (Giblin and Kelly, 2001; Shimaoka et al., 2002).

Inside-Out Signaling

Inside-out activation of integrins occurs as a result of breakage of interactions between the membrane proximal regions of the α and β subunits (Hughes et al., 1996; Lu et al., 2001b; Takagi et al., 2001; Vinogradova et al., 2002). The talin head domain can directly activate integrins by binding to the β subunit cytoplasmic domain (Vinogradova et al., 2002). In the crystal structure, the most C-terminal, membrane proximal residues of αV and β3 are very close to one another (Xiong et al., 2001), as appropriate for a low affinity conformation with interacting membrane proximal segments. We found that the C-terminal clasp stabilized the bent conformation relative to the extended conformation, and stabilized the extended conformation with a closed headpiece relative to the extended conformation with an open headpiece. These findings support the model that movement apart of the membrane proximal segments of the α and β subunits is a mechanism for integrin activation in inside-out signaling (Figure 6C). In the αVβ3 crystal structure, the lower legs of the α and β subunits, i.e., the portions below the bend at the genu, have substantial interactions with one another, and in turn the lower β leg has a prominent role in the headpiece-tailpiece interface (Table 2). Therefore, destabilizing the conformation of the lower β leg by breakage of its interaction with the lower α leg would also destabilize the headpiece-tailpiece interface and favor a switchblade-like opening of this interface. This provides a mechanism for communicating conformational change from the membrane to the headpiece.

The Headpiece-Tailpiece and α Tailpiece-β Tailpiece Interfaces in Integrin Activation

The headpiece-tailpiece and α tailpiece-β tailpiece interfaces each bury over 2000 $Å^2$ of solvent accessible surface (Table 2). The unusually large area by the standards of protein-protein interfaces (Conte et al., 1999) of each of these interfaces suggests biological importance in integrin function, in agreement with their critical role defined here in regulating integrin activation. These two interfaces would be even larger if the PSI, I-EGF-1, I-EGF-2, and the complete I-EGF-3 domains had been resolved, which locate to the bend in the β subunit and nestle close to the bend in the α subunit (Beglova et al., 2002). The combined size of the two interfaces of 4,400 $Å^2$ is greater than the size of the interface between the α and β subunits in the headpiece (Table 2).

Our electron microscopic studies show that when the headpiece-tailpiece interface is broken, the α tailpiece-β tailpiece interface is also broken. The α subunit adopts a fairly uniform orientation in the extended conformation, showing that the genu snaps into a stable alternative conformation after unbending and that the other interdomain interfaces in the α leg are stable. However, in the extended conformation, the lower β leg exists in many alternative conformations, and disappeared in most projection averages. In the clasp, a flexible linker with a TEV cleavage site intervenes between the coiled-

coil and the C terminus of the β leg, and therefore it is not surprising that the clasp did not orient the lower β leg. Throughout their lengths, no association between the α and β legs was seen in extended integrins, with the exception of occasional crossing of the legs in the closed conformation of the headpiece, which may be a consequence of the acute angle that the hybrid domain makes with regard to the head rather than association between the legs. Therefore, breaking the headpiece-tailpiece interface also destabilizes the α tailpiece-β tailpiece interface. Because the headpiece-tailpiece and α tailpiece-β tailpiece interfaces are similar in size and complementarity, we expect that breakage of the α tailpiece-β tailpiece interface would also destabilize the headpiece-tailpiece interface.

While we have shown that destabilization of these two interfaces is linked, inside-out signaling should first destabilize the α tailpiece-β tailpiece interface (Figure 6C), and ligand binding should first destabilize the headpiece-tailpiece interface (Figure 6B). We hypothesize that after ligand binding to the bent αVβ3 conformation, rearrangement to a higher-affinity binding site causes the β hybrid domain to swing out and disrupt first the tailpiece-headpiece interface (Figure 6B) and then the α tailpiece-β tailpiece interface; ligand binding directly induces the extended, open conformation (Figure 6E). Inside-out signaling should favor the intermediate conformation (Figure 6D), which should be sufficient to enhance affinity for ligand. A series of linked equililbria between the three integrin conformers defined here explain how inside-out signaling and ligand binding can both favor the extended conformation, and conversely, how maintenance of close association between the juxtamembrane segments of the α and β subunits stabilizes the bent conformation (Figure 6A). It is significant that the hybrid domain has by far the greatest surface area buried in the headpiece-tailpiece interface (Table 2). This design is ideal to couple maintenance of the headpiece-tailpiece interface to maintenance of the hybrid domain-I-like domain interface in the acute orientation, which is associated with low affinity for ligand.

The flexibility of the lower β leg illustrates the difficulty of transmitting conformational signals through long, extended structures. Other surface receptors that transmit signals have ligand binding sites that are much closer to the membrane (Falke and Hazelbauer, 2001; Remy et al., 1999). Transition between bent and extended conformations in integrins provides a solution to the problem of signal transmission over long distances. It enables an active ligand binding site to be displayed far above the surface of a cell, while equilibration with a bent, inactive conformation enables signals between the ligand binding site and the cytoplasmic domains to be relayed over relatively short distances to protein interfaces present in the bent conformation. Our findings should put to rest the controversy over whether integrin conformational change enables ligand binding or is a consequence of ligand binding (Bazzoni and Hemler, 1998), because they suggest that both inside-out and outside-in signals destabilize the bent conformation. This finding is highly consistent with the fact that ligand binding to integrins and inside-out activation of integrins induce an overlapping or even identical set of epitopes.

Movement at the I-like Domain-Hybrid Domain Interface in Integrin Activation

One of our most striking observations is the obtuse orientation of the hybrid domain relative to the I-like domain seen in the extended conformation with the open headpiece. This conformation corresponds to the high affinity, ligand-bound state of integrins. The obtuse orientation of the hybrid domain is unequivocally distinct from the acute orientation seen in the αVβ3 crystal structure. Therefore, a conformational change occurs at the I-like domain-hybrid domain interface upon conversion to the high affinity state. The I and I-like domains are each connected through both their N and C termini to the domains in which they are inserted, the β propeller and hybrid domains, respectively (Figure 1). We modeled a downward movement of the C-terminal α-helix of the I-like domain that is analogous to that seen in I domain activation and found that it would pivot the hybrid domain away from the α subunit about a fulcrum at the N terminus of the I-like domain, and open the headpiece. Our finding of conformational rearrangement at the I-like domain-hybrid domain interface is consistent with its relatively small size of 650 Å^2 (Xiong et al., 2001) and the predominance of hydrogen bond contacts; allosteric transitions are generally mediated by rearrangement of hydrogen bond rather than hydrophobic contacts at subunit or domain interfaces (Perutz, 1989). In I domains, rearrangement of the MIDAS into the ligand binding configuration is tightly coupled to downward movement of the C-terminal α-helix (Shimaoka et al., 2002). In the crystal structure of the complex of cyclo-RGDf-mV with αVβ3, a similar rearrangement around the MIDAS of the I-like domain appears to have begun, with an inward movement of the α1-helix (Xiong et al., 2002). In I domains, this "squeezes" the hydrophobic core of the domain and pops out nearby residues in the turn preceding the C-terminal α helix, pushing it down the side of the domain. However, completion of this process with an analogous downward movement of the C-terminal α helix in the I-like domain, coupled to swing-out of the hybrid domain, would be frustrated in the co-crystal by the extensive contacts of the hybrid domain with the tailpiece and by lattice contacts that prevent adoption of the extended conformation.

The EM projection averages demonstrate swing-out of the hybrid domain in the ligand-bound, open configuration of the headpiece. They do not define the underlying detailed structural rearrangements; for example, we cannot distinguish unwinding of a portion of the C-terminal α helix from a rigid body movement of this helix. However, alternative movements such as unwinding do not provide a mechanism for coupling cyclo-RGDfV binding at the top of the I-like domain to hybrid domain swing-out at the bottom of the I-like domain, which the EM studies clearly establish. Since such a coupling mechanism has already been demonstrated in structurally homologous I domains (Shimaoka et al., 2002), we can confidently predict that a similar downward C-terminal α helix movement is also coupled to rearrangements in the binding site at the MIDAS in I-like domains that increase affinity for ligand. The structural rearrangements reported here enable important insights into the mechanisms underlying inside-out and outside-in signaling in the extracellular portion of integrins. It will be interesting

to confirm and extend this work with mutational studies on the inter-domain linkage mechanisms, and with crystal and high-resolution EM structures of integrin-ligand complexes that are not constrained in the bent conformation.

Experimental Procedures

Production of Soluble Recombinant αVβ3

Soluble, clasped αV (αV-AHCys) and β3 (β3-tev-BHCys) constructs were prepared from wild-type human αV and β3 cDNAs by overlap extension PCR using the same design as for soluble clasped α5β1 (Takagi et al., 2001), except that a hexahistidine tag was fused to the C terminus of β3. Soluble integrin was purified from culture supernatant of stably transfected CHO lec 3.2.8.1 cells using Ni-NTA agarose (QIAGEN) followed by anion-exchange (monoQ) and gel filtration (Superdex 200 HR) chromatographies. The final preparation was devoid of aggregated materials and eluted as a single peak around 300 kDa, and was stored at 0.5–1 mg/ml at 4°C in 50 mM Tris HCl (pH 7.5), 150 mM NaCl (TBS), containing 1mM $CaCl_2$ and 1 mM $MgCl_2$. Release of the C-terminal clasp of αVβ3 was achieved by incubation with 250 U/ml TEV protease (Invitrogen) at 25°C for 16 hr.

Gel Filtration

Purified clasped or unclasped αVβ3 was incubated in TBS containing the specified divalent cations, in the presence or absence of 60 μM cyclo-RGDfV (Bachem Bioscience, Inc.) at room temperature for 30 min. Samples were injected into a Superdex 200HR 10/30 column (Amersham Pharmacia) connected to an AKTA FPLC system at a flow rate of 0.75ml/min. Columns were pre-equilibrated as appropriate with divalent cations and cyclo-RGDfV (1 μM).

Electron Microscopy and Image Processing

Peak fractions from gel filtration were immediately adsorbed to glow-discharged (negatively charged) carbon-coated copper grids. Grids were washed with two drops of deionized water and stained with two drops of freshly prepared 0.75% uranyl formate. Specimens were inspected with a Philips Tecnai 12 electron microscope operated at 120 kV and images were recorded at a nominal magnification of 52,000× using low-dose procedures. Images were digitized with a Zeiss SCAI scanner using a step size of 7 μm and 3 × 3 pixels were averaged to yield a final pixel size of 4 Å at the specimen level. Particles were windowed into smaller images of 100 × 100 pixels, aligned to each other, and classified into groups specifying 50 output classes using the multi-reference alignment procedure. The particles in each class were then averaged to produce individual class averages. For comparison with the X-ray structures, the X-ray models were resolution-filtered to 25 Å and projections were calculated at an angular interval of 2 degrees. These re-projections were cross-correlated to selected class averages (Figures 3A, 3C, and 3E) and the re-projections with the highest correlation coefficient selected for Figures 3B, 3D, and 3F. All image processing steps were carried out with SPIDER (Frank et al., 1996).

Surface Plasmon Resonance

Experiments were performed using the BIAcore 1000 (Biacore AB). Dilutions of αVβ3 in TBS containing either 1 mM $MnCl_2$ or 1 mM $CaCl_2$ and 1 mM $MgCl_2$ were injected over 6 min at 10 μl/min into flow cells containing either ~8000 RU of human fibrinogen (Enzyme Research Laboratories) or ~6000 RU of native monomeric human vitronectin (gift from D.F. Mosher) coupled to a sensor chip CM5. After each cycle of association/dissociation, the surface was regenerated by injecting 30 μl of 20 mM EDTA, 1M NaCl, and 50 mM Tris (pH 7.5). This treatment did not affect the subsequent binding reaction after up to 20 repetitions.

Expression and Ligand Binding Activity of Integrin on the Cell Surface

Full-length human β3 cDNA was transferred to pcDNA3.1/Myc (Invitrogen) so that the C terminus was in-frame with the Myc and hexahistidine tags. Full-length human αV and αIIb cDNAs were transferred to pEF1/V5-His (Invitrogen) so that the C terminus was in-frame with the V5 tag. Cysteine mutations (G307C in αV, R320C in αIIb, and R563C in β3) were made by site-directed mutagenesis. Mutant as well as wild-type integrin subunits were transiently transfected into 293T cells using calcium phosphate precipitates. Binding of FITC-fibrinogen was determined as previously described (Pampori et al., 1999). Activating mAbs AP5 (Fifth International Leukocyte Workshop) and PT25-2 (gift from M. Handa,) were used at 1:50 ascites and 7.5 μg/ml, respectively. After a final staining with Cy3-labeled AP3 (nonfunctional anti-β3 mAb, American Type Culture Collection), the β3-positive cell population was analyzed for the binding of FITC-fibrinogen.

Acknowledgments

The authors thank Drs. S.J. Shattil, D.F. Mosher, and M. Handa for generous gifts, D.P. DeBottis for technical assistance, and Dr. T. Xiao for help with computation. The present study was supported by NIH grant HL48675 (to T.A.S. and J.T).

The molecular electron microscopy facility at Harvard Medical School was established with a generous donation from the Giovanni Armenise Harvard Center for Structural Biology and is maintained by funds from NIH grant GM62580.

Received: May 24, 2002
Revised: August 20, 2002
Published online: August 30, 2002

References

Bailey, S. (1994). The CCP4 suite-programs for protein crystallography. Acta Crystallogr. D Biol. Crystallogr. *50*, 760–763.

Bazzoni, G., and Hemler, M.E. (1998). Are changes in integrin affinity and conformation overemphasized? Trends Biochem. Sci. *23*, 30–34.

Bazzoni, G., Ma, L., Blue, M.-L., and Hemler, M.E. (1998). Divalent cations and ligands induce conformational changes that are highly divergent among β1 integrins. J. Biol. Chem. *273*, 6670–6678.

Bednar, B., Cunningham, M.E., McQueney, P.A., Egbertson, M.S., Askew, B.C., Bednar, R.A., Hartman, G.D., and Gould, R.J. (1997). Flow cytometric measurement of kinetic and equilibrium binding parameters of arginine-glycine-aspartic acid ligands in binding to glycoprotein IIb/IIIa on platelets. Cytometry *28*, 58–65.

Beglova, N., Blacklow, S.C., Takagi, J., and Springer, T.A. (2002). Cysteine-rich module structure reveals a fulcrum for integrin rearrangement upon activation. Nat. Struct. Biol. *9*, 282–287.

Billheimer, J.T., Dicker, I.B., Wynn, R., Bradley, J.D., Cromley, D.A., Godonis, H.E., Grimminger, L.C., He, B., Kieras, C.J., Pedicord, D.L., et al. (2002). Evidence that thrombocytopenia observed in humans treated with orally bioavailable glycoprotein IIb/IIIa antagonists is immune mediated. Blood *99*, 1–7.

Brooks, P.C., Montgomery, A.M., Rosenfeld, M., Reisfeld, R.A., Hu, T., Klier, G., and Cheresh, D.A. (1994). Integrin αVβ3 antagonists promote tumor regression by inducing apoptosis of angiogenic blood vessels. Cell *79*, 1157–1164.

Coller, B.S. (2001). Anti-GPIIb/IIIa drugs: current strategies and future directions. Thromb. Haemost. *86*, 427–443.

Conte, L.L., Chothia, C., and Janin, J. (1999). The atomic structure of protein-protein recognition sites. J. Mol. Biol. *285*, 2177–2198.

Dechantsreiter, M.A., Planker, E., Matha, B., Lohof, E., Holzemann, G., Jonczyk, A., Goodman, S.L., and Kessler, H. (1999). N-Methylated cyclic RGD peptides as highly active and selective αVβ3 integrin antagonists. J. Med. Chem. *42*, 3033–3040.

Du, X., Plow, E.F., Frelinger, A.L., III, O'Toole, T.E., Loftus, J.C., and Ginsberg, M.H. (1991). Ligands "activate" integrin αIIbβ3 (platelet GPIIb-IIIa). Cell *65*, 409–416.

Du, X., Gu, M., Weisel, J.W., Nagaswami, C., Bennett, J.S., Bowditch, R., and Ginsberg, M.H. (1993). Long range propagation of conformational changes in integrin $\alpha_{IIb}\beta_3$. J. Biol. Chem. *268*, 23087–23092.

Egbertson, M.S., Cook, J.J., Bednar, B., Prugh, J.D., Bednar, R.A., Gaul, S.L., Gould, R.J., Hartman, G.D., Homnick, C.F., Holahan, M.A.,

et al. (1999). Non-peptide GPIIb/IIIa inhibitors. 20. Centrally constrained thienothiophene alpha-sulfonamides are potent, long acting in vivo inhibitors of platelet aggregation. J. Med. Chem. *42*, 2409–2421.

Falke, J.J., and Hazelbauer, G.L. (2001). Transmembrane signaling in bacterial chemoreceptors. Trends Biochem. Sci. *26*, 257–265.

Frank, J., Radermacher, M., Penczek, P., Zhu, J., Li, Y., Ladjadj, M., and Leith, A. (1996). SPIDER and WEB: processing and visualization of images in 3D electron microscopy and related fields. J. Struct. Biol. *116*, 190–199.

Frelinger, A.L., Cohen, I., Plow, E.F., Smith, M.A., Roberts, J., Lam, S.C.T., and Ginsberg, M.H. (1990). Selective inhibition of integrin function by antibodies specific for ligand-occupied receptor conformers. J. Biol. Chem. *265*, 6346–6352.

Giancotti, F.G., and Ruoslahti, E. (1999). Integrin signaling. Science *285*, 1028–1032.

Giblin, P.A., and Kelly, T.A. (2001). Antagonists of β2 integrin-mediated cell adhesion. Annu. Rep. Med. Chem. *36*, 181–190.

Hemler, M.E. (1998). Integrin associated proteins. Curr. Opin. Cell Biol. *10*, 578–585.

Huber, W., Hurst, J., Schlatter, D., Barner, R., Hübscher, J., Kouns, W.C., and Steiner, B. (1995). Determination of kinetic constants for the interaction between the platelet glycoprotein IIb-IIIa and fibrinogen by means of surface plasmon resonance. Eur. J. Biochem. *227*, 647–656.

Hughes, P.E., and Pfaff, M. (1998). Integrin affinity modulation. Trends Cell Biol. *8*, 359–364.

Hughes, P.E., Diaz-Gonzalez, F., Leong, L., Wu, C., McDonald, J.A., Shattil, S.J., and Ginsberg, M.H. (1996). Breaking the integrin hinge. J. Biol. Chem. *271*, 6571–6574.

Kouns, W.C., Kirchhofer, D., Hadvary, P., Edenhofer, A., Weller, T., Pfenninger, G., Baumgartner, H.R., Jennings, L.K., and Steiner, B. (1992). Reversible conformational changes induced in glycoprotein IIb-IIIa by a potent and selective peptidomimetic inhibitor. Blood *80*, 2539–2547.

Legler, D.F., Wiedle, G., Ross, F.P., and Imhof, B.A. (2001). Superactivation of integrin αVβ3 by low antagonist concentrations. J. Cell Sci. *114*, 1545–1553.

Liu, S., Calderwood, D.A., and Ginsberg, M.H. (2000). Integrin cytoplasmic domain-binding proteins. J. Cell Sci. *113*, 3563–3571.

Lu, C., Ferzly, M., Takagi, J., and Springer, T.A. (2001a). Epitope mapping of antibodies to the C-terminal region of the integrin β2 subunit reveals regions that become exposed upon receptor activation. J. Immunol. *166*, 5629–5637.

Lu, C., Takagi, J., and Springer, T.A. (2001b). Association of the membrane-proximal regions of the α and β subunit cytoplasmic domains constrains an integrin in the inactive state. J. Biol. Chem. *276*, 14642–14648.

Marvin, J.S., and Hellinga, H.W. (2001). Manipulation of ligand binding affinity by exploitation of conformational coupling. Nat. Struct. Biol. *8*, 795–798.

Nermut, M.V., Green, N.M., Eason, P., Yamada, S.S., and Yamada, K.M. (1988). Electron microscopy and structural model of human fibronectin receptor. EMBO J. *7*, 4093–4099.

Pampori, N., Hato, T., Stupack, D.G., Aidoudi, S., Cheresh, D.A., Nemerow, G.R., and Shattil, S.J. (1999). Mechanisms and consequences of affinity modulation of integrin αVβ3 detected with a novel patch-engineered monovalent ligand. J. Biol. Chem. *274*, 21609–21616.

Parise, L.V., Helgerson, S.L., Steiner, B., Nannizzi, L., and Phillips, D.R. (1987). Synthetic peptides derived from fibrinogen and fibronectin change the conformation of purified platelet glycoprotein IIb-IIIa. J. Biol. Chem. *262*, 12597–12602.

Perutz, M.F. (1989). Mechanisms of cooperativity and allosteric regulation in proteins. Q. Rev. Biophys. *22*, 139–237.

Peter, K., Schwarz, M., Ylanne, J., Kohler, B., Moser, M., Nordt, T., Salbach, P., Kubler, W., and Bode, C. (1998). Induction of fibrinogen binding and platelet aggregation as a potential intrinsic property of various glycoprotein IIb/IIIa (αIIbβ3) inhibitors. Blood *92*, 3240–3249.

Remy, I., Wilson, I.A., and Michnick, S.W. (1999). Erythropoietin receptor activation by a ligand-induced conformation change. Science *283*, 990–993.

Scarborough, R.M., and Gretler, D.D. (2000). Platelet glycoprotein IIb-IIIa antagonists as prototypical integrin blockers: novel parenteral and potential oral antithrombotic agents. J. Med. Chem. *43*, 3453–3473.

Schwartz, M.A., and Ginsberg, M.H. (2002). Networks and crosstalk: integrin signalling spreads. Nat. Cell Biol. *4*, E65–E68.

Shimaoka, M., Takagi, J., and Springer, T.A. (2002). Conformational regulation of integrin structure and function. Annu. Rev. Biophys. Biomol. Struct. *31*, 485–516.

Smith, J.W., Piotrowicz, R.S., and Mathis, D. (1994). A mechanism for divalent cation regulation of β3-integrins. J. Biol. Chem. *269*, 960–967.

Takagi, J., Erickson, H.P., and Springer, T.A. (2001). C-terminal opening mimics "inside-out" activation of integrin α5β1. Nat. Struct. Biol. *8*, 412–416.

Tanford, C. (1961). Physical Chemistry of Macromolecules, First Edition. (New York: Wiley and Sons, Inc.).

Vinogradova, O., Velyvis, A., Velyviene, A., Hu, B., Haas, T.A., Plow, E.F., and Qin, J. (2002). A structural mechanism of integrin $\alpha_{IIb}\beta_3$ "inside-out" activation as regulated by its cytoplasmic face. Cell *110*, this issue, 587–597.

Xiong, J.-P., Stehle, T., Diefenbach, B., Zhang, R., Dunker, R., Scott, D.L., Joachimiak, A., Goodman, S.L., and Arnaout, M.A. (2001). Crystal structure of the extracellular segment of integrin αVβ3. Science *294*, 339–345.

Xiong, J.P., Stehle, T., Zhang, R., Joachimiak, A., Frech, M., Goodman, S.L., and Arnaout, M.A. (2002). Crystal structure of the extracellular segment of integrin αVβ3 in complex with an Arg-Gly-Asp ligand. Science *295*, 151–155.

Yan, B., and Smith, J.W. (2001). Mechanism of integrin activation by disulfide bond reduction. Biochemistry *40*, 8861–8867.

Zang, Q., and Springer, T.A. (2001). Amino acid residues in the PSI domain and cysteine-rich repeats of the integrin β2 subunit that restrain activation of the integrin αXβ2. J. Biol. Chem. *276*, 6922–6929.